A Stochastic Filtering Technique for Fluid Flow Velocity Fields Tracking

Anne Cuzol and Etienne Mémin

Abstract—In this paper, we present a method for the temporal tracking of fluid flow velocity fields. The technique we propose is formalized within a sequential Bayesian filtering framework. The filtering model combines an Itô diffusion process coming from a stochastic formulation of the vorticity-velocity form of the Navier-Stokes equation and discrete measurements extracted from the image sequence. In order to handle a state space of reasonable dimension, the motion field is represented as a combination of adapted basis functions, derived from a discretization of the vorticity map of the fluid flow velocity field. The resulting nonlinear filtering problem is solved with the particle filter algorithm in continuous time. An adaptive dimensional reduction method is applied to the filtering technique, relying on dynamical systems theory. The efficiency of the tracking method is demonstrated on synthetic and real-world sequences.

Index Terms—Motion estimation, tracking, nonlinear stochastic filtering, fluid flows.

1 Introduction

The analysis and understanding of image sequences involving fluid phenomena has important real-world applications. Let us cite, for instance, the domain of geophysical sciences, such as meteorology and oceanography, where one wants to track atmospheric systems for weather forecasting or for surveillance purposes, estimate ocean streams, or monitor the drift of passive entities such as icebergs or pollutant sheets. The analysis of geophysical flows from satellite images is of particular interest in large regions of the world, such as Africa or the Southern hemisphere, which face a very sparse network of meteorological stations. A more intensive use of satellite images might provide these lacking information. Images also have a finer spatial and temporal resolution than the large-scale dynamical models used for weather forecasting. Image data then offers richer information on small motion scales. However, the analysis of flow quantities is an intricate issue as the sought quantities are only indirectly observed on a 2D plan through a luminance function. Because of this difficulty, satellite images are very poorly used in forecasting models.

The analysis of fluid flow images is also crucial in experimental fluid mechanics in order to analyze flows around wing tips or vortex shedding from airfoils or cylinders. Such an analysis allows us to get dense velocity measurements by way of nonintrusive sensors. This enables fluid mechanics in particular to have a better understanding of some phenomena occurring in complex fluid flows or to settle specific actions in view of flow control. This last problem is a major industrial issue for several application domains and such control is hardly conceivable without having access to kinematical or dynamical measurements of the flow. Imaging sensors and motion analysis provide a convenient way to get these measurements.

For the analysis of complex flows interactions like those encountered between fluid and structures, in sea-atmosphere interactions, dispersion of polluting agents in seas and rivers, or for the study of flows involving complex unknown border conditions, image data might be a very interesting alternative to a pure dynamical modeling in order to extract quantitative flow features of interest. To that end, the knowledge developed in computer vision for video sequence analysis, 3D reconstruction, machine learning, or visual tracking is extremely precious and unavoidable. However, the direct application of such general frameworks are likely to fail in a fluid context, mainly because of the highly nonlinear nature of fluid dynamics, which involves a coupling of a broad range of spatial and temporal scales of the phenomenon. In this context, it is necessary to invent techniques allowing the association of a fluid dynamical modeling and image observations of the flows. The study proposed here is a first attempt at such an issue.

For all of the aforementioned applications and domains, it is of major interest to track along time, as accurately as possible, representative structures of the flow. Such a temporal tracking may be obtained from deterministic integration methods, such as the Euler method or the Runge and Kutta integration technique, from successive independent motion estimates. These numerical integration approaches rely on a continuous spatiotemporal vector field description and, thus, require the use of interpolation schemes over the whole spatial and temporal domain of interest. As a consequence, they are quite sensitive to local errors in measurements or to inaccurate motion estimates. When the images are noisy or if the flow velocities are of high magnitude and chaotic as, for instance, in the case of

- *A. Cuzol is with the European University of Brittany-UBS, CNRS UMR 3192-Lab-STICC, Campus de Tohannic, BP 573, F-56000 Vannes Cedex, France. E-mail: anne.cuzol@univ-ubs.fr.*
- *E. Mémin is with Centre INRIA Rennes-Bretagne Atlantique, Campus Universitaire de Beaulieu, 35042 Rennes Cedex, France. E-mail: Etienne.Memin@inria.fr.*

Manuscript received 7 Jan. 2007; revised 12 Jan. 2008; accepted 12 May 2008; published online 4 June 2008.
Recommended for acceptance by J. Weikert.
For information on obtaining reprints of this article, please send e-mail to: tpami@computer.org, and reference IEEECS Log Number TPAMI-0006-0107.
Digital Object Identifier no. 10.1109/TPAMI.2008.152.

turbulent flows, motion estimation tends to be quite difficult and prone to errors. Another major difficulty in motion estimation is the temporal consistency between estimates. This problem is inherent in motion estimation techniques (see, for instance, [3] for an extended review on motion estimation techniques). As a matter of fact, most of the motion estimation approaches use only a small set of images (usually two consecutive images of a sequence) and thus may suffer from a temporal inconsistency from frame to frame. The extension of spatial regularizers to spatio-temporal regularizers [36] or the introduction of simple dynamical constraints in motion segmentation techniques relies mainly on crude dynamic assumptions or are related to rigid object motion only [19].

Some recent contributions [20], [29], [30], [34] aim at improving the temporal consistency and the robustness of the estimations over the whole sequence, introducing a physical evolution law in the estimation process. The dense motion estimation methods dedicated to fluid flows, based on a spatial regularization of the vector fields, have been extended to integrate temporal constraints related to the fluid flow evolution [22], [35], [33]. These constraints are either derived from the vorticity-velocity formulation of the Navier-Stokes equation [22], [35] or from the Stokes equation [33]. Recent techniques based on variational tracking methods rely on similar dynamical models [29], [30]. In that case, the temporal tracking is based on an optimal control concept. Successive noisy estimations of the vector fields are then smoothed and corrected according to the considered conservation law. One advantage of the variational tracking method is that the state vector of the system can be of very high dimension. However, a restriction is that this approach relies on a Gaussian assumption, in the same spirit as a Kalman smoother.

We choose here to formulate the temporal tracking as a stochastic filtering problem. The objective of stochastic filtering (presented in Section 2) is to estimate the state of a time-varying system, indirectly observed through noisy measurements. The target of interest is described by random vector variables, evolving following a state equation. The state can evolve in discrete or continuous time. The typical situation in image analysis is to describe the evolution of a state with a discrete time model, where the time step corresponds to the image time step. Autoregressive models or data-driven dynamic models are the most frequently used when the information about the underlying dynamical law is poor or is estimated from the images.

If the phenomena of interest are continuous by nature, a continuous dynamical model is a more realistic approach. Such continuous dynamics describing the evolution of the state vector of interest in the image plane may be derived from physical conservation laws. These laws may be perfectly reproduced if their expressions are simple, or approximated up to an uncertainty, modeled as a noise term. The description of the state model from such a continuous evolution law is then the better way to reproduce faithfully the nature of the phenomena. Moreover, abrupt changes can be observed between two distant observations if the evolution of the state is very nonlinear or chaotic. A continuous dynamical model may then be more adapted to take into account a long interval of time between two measurements. This is the case for fluid flows, as they are associated to a highly nonlinear and continuous evolution law by nature. Note that the observation process may also be considered as continuous if the time step between observations is small enough. However, for observations coming from image sequences, the measurements are supposed to be given at discrete time instants. In addition, the time step between two observations can be quite long (in meteorological or oceanographic applications for instance).

The choice of a probabilistic approach enables us to cope with any nonlinearity in the evolution model and to deal with a nonlinear relation between the state and the measurements extracted from the images. The general stochastic filtering problem does not rely on any Gaussian assumption or linearity of the model. However, the filtering problem associated to such nonlinear models does not have any explicit analytical solution and is usually difficult to implement numerically for a high-dimensional state vector. As a matter of fact, Monte-Carlo probabilistic tracking methods as proposed in the literature [17], [23], [31] are efficient to track objects of reduced dimension such as points or curves described by several discrete control points. These techniques are not able to cope with high-dimensional features such as dense vector fields. In our work, in order to handle motion fields of reasonable dimension, we rely on an original parameterization of fluid flows [15], [13] relying on adequate basis functions. The used basis functions stem from Biot-Savart integration of a regularized discretization of the vector field vorticity and divergence maps [7], [12]. Such a representation enables a reduced-size representation of a fluid motion. The second difficulty is related to the continuous nature of the involved dynamic evolution law. The problem thus consists of the definition of an appropriate sequential Monte-Carlo approximation of a stochastic filter which combines a continuous dynamical law expressed as a stochastic differential equation and discrete measurements extracted from the image sequence.

This paper is organized as follows: The stochastic filtering problem is presented in Section 2. In particular, the principle of a continuous nonlinear filtering with an appropriate continuous version of the particle filter algorithm is exposed. The construction of the filtering model we propose to solve the fluid flow velocity fields tracking problem is presented in Section 3. We then present in Section 4 the application of an adaptive dimensional reduction method to our high-dimensional tracking problem, relying on dynamical systems theory. The last section shows tracking results for synthetic and real examples, with applications in experimental fluid mechanics and meteorology. This paper extends a previous conference paper [14].

2 Stochastic Filtering Problem

We present in this section the stochastic filtering problem in continuous time with discrete observations. The particle filter for the discrete case is recalled and its continuous time version is presented.

2.1 Filtering Model

The random vector $\mathbf{x}$ describes the state characteristics and the observations are denoted by $\mathbf{z}$. The state process $(\mathbf{x}_t)_{t\geq t_0}$ evolves in continuous time according to a stochastic differential equation. The observations $(\mathbf{z}_{t_k})_{t_k\geq t_1}$ are given at time instants t_k and form a discrete process. At each time t_k, the measurement equation relates the observation $\mathbf{z}_{t_k}$ to the state $\mathbf{x}_{t_k}$. The corresponding state space model is described by

$$\begin{cases} d\mathbf{x}_t &= f(\mathbf{x}_t)dt + \sigma(\mathbf{x}_t)d\mathbf{B}_t, \\ \mathbf{z}_{t_k} &= g(\mathbf{x}_{t_k}) + \mathbf{v}_{t_k}, \end{cases} \quad (1)$$

where $f(\mathbf{x}_t)$ is the deterministic drift term of the stochastic differential equation, $\sigma(\mathbf{x}_t)$ is the diffusion term relative to the Brownian motion $\mathbf{B}_t$, and $\mathbf{v}_{t_k}$ is a given noise. The functions f and g are nonlinear in the general case.

2.2 Optimal Filtering

The optimal filtering solution computes the filtering distribution $p(\mathbf{x}_{t_k}|\mathbf{z}_{t_1:t_k})$ at each measurement time t_k. This distribution can be obtained recursively by the Bayesian filtering equations. Indeed, assuming $p(\mathbf{x}_{t_{k-1}}|\mathbf{z}_{t_1:t_{k-1}})$ is known, the filtering distribution $p(\mathbf{x}_{t_k}|\mathbf{z}_{t_1:t_k})$ is evaluated in two steps:

- The **prediction step** evaluates the predicted filtering distribution $p(\mathbf{x}_{t_k}|\mathbf{z}_{t_1:t_{k-1}})$ from $p(\mathbf{x}_{t_{k-1}}|\mathbf{z}_{t_1:t_{k-1}})$ and the transition distribution $p(\mathbf{x}_{t_k}|\mathbf{x}_{t_{k-1}})$:

$$p(\mathbf{x}_{t_k}|\mathbf{z}_{t_1:t_{k-1}}) = \int p(\mathbf{x}_{t_k}|\mathbf{x}_{t_{k-1}})p(\mathbf{x}_{t_{k-1}}|\mathbf{z}_{t_1:t_{k-1}})d\mathbf{x}_{t_{k-1}}. \quad (2)$$

- The **correction step** integrates the new observation $\mathbf{z}_{t_k}$ through the knowledge of the likelihood $p(\mathbf{z}_{t_k}|\mathbf{x}_{t_k})$. The filtering distribution is then updated in the following way:

$$p(\mathbf{x}_{t_k}|\mathbf{z}_{t_1:t_k}) = \frac{p(\mathbf{z}_{t_k}|\mathbf{x}_{t_k})p(\mathbf{x}_{t_k}|\mathbf{z}_{t_1:t_{k-1}})}{\int p(\mathbf{z}_{t_k}|\mathbf{x}_{t_k})p(\mathbf{x}_{t_k}|\mathbf{z}_{t_1:t_{k-1}})d\mathbf{x}_{t_k}}. \quad (3)$$

Note that the update step is performed at the measurements times t_k only. Between two consecutive measurement times t_{k-1} and t_k, the filtering distribution can be defined by its predicted form $p(\mathbf{x}_t|\mathbf{z}_{t_1:t_{k-1}})$ for $t_{k-1} < t < t_k$, where $p(\mathbf{x}_t|\mathbf{z}_{t_1:t_{k-1}}) = \int p(\mathbf{x}_t|\mathbf{x}_{t_{k-1}})p(\mathbf{x}_{t_{k-1}}|\mathbf{z}_{t_1:t_{k-1}})d\mathbf{x}_{t_{k-1}}$.

2.3 Particle Filter

In the case of a linear state model and a linear and Gaussian measurement model, the closed-form solution of the filtering problem is known. The filtering problem is solved with the Kalman filter. For the nonlinear case, the exact solution of the optimal filtering equations is not available. For weak nonlinearities, the filtering distributions can be approximated by a Gaussian. However, this approximation is too restrictive for most of the tracking problems in vision. A better choice is to use a Monte-Carlo approximation of the filtering density:

$$p(\mathbf{x}_{t_k}|\mathbf{z}_{t_1:t_k}) \approx \sum_{i=1}^{\mathrm{N}} w_{t_k}^{(i)} \delta_{\mathbf{x}_{t_k}^{(i)}}(\mathbf{x}_{t_k}), \quad (4)$$

where $\delta_{\mathbf{x}_{t_k}^{(i)}}(\mathbf{x}_{t_k})$ denotes the delta measure centered on $\mathbf{x}_{t_k}^{(i)}$, which means that $\delta_{\mathbf{x}_{t_k}^{(i)}}(\mathbf{x}_{t_k}) = 1$ if $\mathbf{x}_{t_k} = \mathbf{x}_{t_k}^{(i)}$, else 0. The weighted set of particles (called *trajectories* in the rest of this paper) $\{\mathbf{x}_{t_k}^{(i)}, w_{t_k}^{(i)}\}_{i=1:\mathrm{N}}$ can be updated and reweighted recursively with the particle filtering method, leading to a recursive Monte-Carlo approximation of the filtering density.

2.3.1 Discrete Time Particle Filter

We briefly recall the particle filter algorithm [17], [23] for the particular case of a fully discrete state space model of the form

$$\begin{cases} \mathbf{x}_k = f(\mathbf{x}_{k-1}) + \mathbf{w}_{k-1}, \\ \mathbf{z}_k = g(\mathbf{x}_k) + \mathbf{v}_k, \end{cases} \quad (5)$$

with $\mathbf{w}_{k-1}$ and $\mathbf{v}_k$ denoting independent noises. During the prediction step, each trajectory is sampled from an approximation of the unknown posterior distribution called the importance distribution. The correction step consists of a recursive evaluation of each weight, using the measurement likelihood:

- **Prediction step** (sampling w.r.t. the importance distribution)

$$\mathbf{x}_k^{(i)} \sim \pi\left(\mathbf{x}_k|\mathbf{x}_{0:k-1}^{(i)}, \mathbf{z}_{1:k}\right) \quad i = 1:\mathrm{N}. \quad (6)$$

- **Correction step and normalization** (taking into account the measurement likelihood)

$$\begin{aligned} w_k^{(i)} &\propto w_{k-1}^{(i)} \frac{p\left(\mathbf{z}_k|\mathbf{x}_k^{(i)}\right)p\left(\mathbf{x}_k^{(i)}|\mathbf{x}_{k-1}^{(i)}\right)}{\pi\left(\mathbf{x}_k^{(i)}|\mathbf{x}_{0:k-1}^{(i)}, \mathbf{z}_{1:k}\right)} \quad \text{and} \\ \widetilde{w}_k^{(i)} &= \frac{w_k^{(i)}}{\sum_{j=1}^{\mathrm{N}} w_k^{(j)}} \quad i = 1:\mathrm{N}. \end{aligned} \quad (7)$$

Note that a resampling step is usually added in order to avoid the degeneracy problem of the set of trajectories. This resampling procedure aims at removing trajectories with small weights and duplicating trajectories with stronger weights. The two steps (6) and (7) together with the resampling of the trajectories form the particle filter. The performance of the algorithm then depends on the choice of the importance distribution $\pi(\mathbf{x}_k|\mathbf{x}_{0:k-1}^{(i)}, \mathbf{z}_{1:k})$. The optimal importance function in terms of variance of the weights is $\pi(\mathbf{x}_k|\mathbf{x}_{0:k-1}^{(i)}, \mathbf{z}_{1:k}) = p(\mathbf{x}_k|\mathbf{x}_{k-1}^{(i)}, \mathbf{z}_k)$ [17]. This optimal function is unfortunately only available for a linear measure equation with Gaussian or mixture of Gaussian likelihood [1]. When such an optimal importance function is not available, the importance function is often simply set to the prediction density [23]: $\pi(\mathbf{x}_k|\mathbf{x}_{0:k-1}^{(i)}, \mathbf{z}_{1:k}) = p(\mathbf{x}_k|\mathbf{x}_{k-1}^{(i)})$. In that case, the recursive formulation of the weights $w_k^{(i)}$ simplifies as

$$w_k^{(i)} \propto w_{k-1}^{(i)} p\left(\mathbf{z}_k|\mathbf{x}_k^{(i)}\right). \quad (8)$$

2.3.2 Continuous-Discrete Time Particle Filter

The particle filter algorithm can be extended to a general continuous model [16]. Indeed, the importance distribution can be fixed to the transition density $p(\mathbf{x}_{t_k}|\mathbf{x}^{(i)}_{t_{k-1}})$ between two observation times t_{k-1} and t_k (as for the bootstrap particle filter [23]). For a general continuous model of the form (1), the prediction and correction steps of the algorithm are then:

- **Prediction step**

$$\mathbf{x}^{(i)}_{t_k} \sim p\Big(\mathbf{x}_{t_k}|\mathbf{x}^{(i)}_{t_{k-1}}\Big) \quad i = 1:\mathrm{N}. \tag{9}$$

- **Correction step and normalization**

$$\begin{aligned} w^{(i)}_{t_k} &\propto w^{(i)}_{t_{k-1}} p(\mathbf{z}_{t_k}|\mathbf{x}^{(i)}_{t_k}) \quad \text{and} \\ \widetilde{w}^{(i)}_{t_k} &= \frac{w^{(i)}_{t_k}}{\sum_{j=1}^{\mathrm{N}} w^{(j)}_{t_k}} \quad i = 1:\mathrm{N}. \end{aligned} \tag{10}$$

The prediction step consists of sampling trajectories $\{\mathbf{x}^{(i)}_t : t_{k-1} \le t \le t_k\}_{i=1:\mathrm{N}}$ from the stochastic differential equation describing the continuous evolution of the state:

$$d\mathbf{x}^{(i)}_t = f(\mathbf{x}^{(i)}_t)dt + \boldsymbol{\sigma}(\mathbf{x}^{(i)}_t)d\mathbf{B}^{(i)}_t, \tag{11}$$

from the initial conditions $\{\mathbf{x}^{(i)}_{t_{k-1}}\}_{i=1:\mathrm{N}}$, where $\{\mathbf{B}^{(i)}_t\}_{i=1:\mathrm{N}}$ are independent Brownian motions. The simulation from the SDE (11) can be done with the Euler scheme or other numerical simulation methods of stochastic differential equations [24]. The Euler scheme has the following form:

$$\mathbf{x}^{(i)}_{t+\Delta t} = \mathbf{x}^{(i)}_t + f\Big(\mathbf{x}^{(i)}_t\Big)\Delta t + \boldsymbol{\sigma}\Big(\mathbf{x}^{(i)}_t\Big)\Big(\mathbf{B}^{(i)}_{t+\Delta t} - \mathbf{B}^{(i)}_t\Big), \tag{12}$$

where the increments $\mathbf{B}^{(i)}_{t+\Delta t} - \mathbf{B}^{(i)}_t$ are independent Gaussian noises with zero mean and variance Δt. Note that the discretization step of the simulation is much smaller than the time step $t_k - t_{k-1}$ between two observations.

The correction step of the filter and the resampling procedure are similar to the discrete case.

3 Construction of the Filtering Model

This section describes the filtering model of type (1) we have settled for the fluid flow velocity fields tracking problem. Considering a dense representation for motion fields constitutes a state space of too high dimension for the particle filtering. As a matter of fact, sampling a probability distribution over such a state space is infeasible in practice. The first task to implement such a filtering approach is to define an appropriate low-dimensional representation of the flow to reduce the complexity of the problem to solve. We describe, in Section 3.1, the low-order representation of fluid flow velocity fields on which we rely in this work. Then, in Section 3.2, the dynamical evolution law associated to this reduced representation of fluid flows is presented. The complete state model we propose for this tracking problem is then defined in Section 3.3. The presentation of the associated measurement model is described in Section 3.4. The global filtering model and the associated continuous particle filter are detailed in Section 3.5.

3.1 Low-Dimensional Representation of Fluid Flows

3.1.1 Two-Dimensional Vector Fields Reminder

A 2D vector field $\mathbf{w}$ is an $\mathbb{R}^2$-valued map defined on a bounded set Ω of $\mathbb{R}^2$. We denote it $\mathbf{w}(\mathbf{x}) = (u(\mathbf{x}), v(\mathbf{x}))^T$, where $\mathbf{x} = (x, y)$ and x and y are the spatial coordinates. The vorticity is defined by $\xi(\mathbf{x}) = \mathrm{curl}\ \mathbf{w}(\mathbf{x}) = \frac{\partial v}{\partial x} - \frac{\partial u}{\partial y}$ and the divergence is defined by $\zeta(\mathbf{x}) = \mathrm{div}\ \mathbf{w}(\mathbf{x}) = \frac{\partial u}{\partial x} + \frac{\partial v}{\partial y}$. The vorticity accounts for the presence of a rotating motion, while the divergence is related to the presence of *sinks* or *sources* in the flow. A vector field that vanishes at infinity can be decomposed into a sum of an *irrotational* component with null vorticity and a *solenoidal* component with null divergence. This is called the *Helmholtz Decomposition* [11], [38]. Let us remark that such a decomposition for a dense motion field can be computed in the Fourier domain [11] or directly specified as a motion estimation problem [37], [38] from the image sequence. When the null border condition cannot be imposed, a *transportation* component, with null vorticity and null divergence, must be included. This component can be approximated using the Horn and Schunck estimator with a strong regularization coefficient [10].

Let us note that the tracking method we propose is adapted to the solenoidal component of vector fields. In the rest of this paper, the vector field $\mathbf{w}$ will then denote the solenoidal part of the flow. The divergent motions, if any, are not tracked and have to be estimated from successive pairs of images. Moreover, we assume that the transportation component is known over the whole sequence.

It is known [11] that $\mathbf{w}(\mathbf{x}) = \boldsymbol{\nabla}^{\perp}\psi(\mathbf{x})$, where ψ is a potential function and $\boldsymbol{\nabla}^{\perp} = (\frac{\partial}{\partial y}, -\frac{\partial}{\partial x})$. The potential function ψ is solution of a Poisson equation: $\Delta\psi(\mathbf{x}) = \xi(\mathbf{x})$, where Δ denotes the Laplacian operator. Let G be the Green's function associated to the Laplacian operator in 2D: $G(\mathbf{x}) = \frac{1}{2\pi}\ln(\|\mathbf{x}\|)$ [9]. The solution ψ is then obtained by convolution

$$\psi(\mathbf{x}) = G * \xi(\mathbf{x}) = \int_{\mathbb{R}^2} G(\mathbf{x} - \mathbf{u})\ \mathrm{curl}\ \mathbf{w}(\mathbf{u})d\mathbf{u}.$$

Finally, $\mathbf{w}(\mathbf{x}) = K * \xi(\mathbf{x})$, where $K(\mathbf{x}) = \boldsymbol{\nabla}^{\perp}G(\mathbf{x}) = \frac{\mathbf{x}^{\perp}}{2\pi\|\mathbf{x}\|^2}$. Note that this relation between the solenoidal component $\mathbf{w}$ and the scalar vorticity ξ is known as the *Biot-Savart integral* [9].

3.1.2 Vorticity Approximation with Vortex Particles

The idea of vortex particles methods [7], [25] consists of representing the vorticity distribution of a field by a set of discrete amounts of vorticity. A discretization of the vorticity into a limited number of elements enables to evaluate the velocity field directly from the Biot-Savart integral. The vorticity is represented by a sum of smoothed Dirac measures, in order to remove the singularities induced by the Green kernel gradient K. The smoothing function is called *cut-off* or *blob* function and is generally a radially symmetric function scaled by a parameter ϵ:

$f_\epsilon(\mathbf{x}) = \frac{1}{\epsilon^2} f(\frac{\mathbf{x}}{\epsilon})$. A vortex particle representation of the vorticity map then reads

$$\xi(\mathbf{x}) \approx \sum_{j=1}^{q} \gamma_j f_{\epsilon_j}(\mathbf{x} - \mathbf{x}_j), \tag{13}$$

where $\mathbf{x}_j$ denotes the center of each basis function f_{ϵ_j}, the coefficient γ_j is the strength associated to the particle, and ϵ_j represents its influence domain. These parameters are free to vary from a function to another. Replacing the vorticity by its approximation (13) into the Biot-Savart integral leads to

$$\mathbf{w}(\mathbf{x}) \approx \sum_{j=1}^{q} \gamma_j K_{\epsilon_j}(\mathbf{x} - \mathbf{x}_j), \tag{14}$$

where K_{ϵ_j} is the smoothed kernel $K_{\epsilon_j} = K * f_{\epsilon_j}$. For some well-chosen cut-off functions, an analytical expression for $\mathbf{w}$ may be obtained [12], [13]. With a Gaussian function for instance, the motion field writes

$$\mathbf{w}_{sol}(\mathbf{x}) \approx \sum_{j=1}^{q} \gamma_j \frac{(\mathbf{x} - \mathbf{x}_j)^\perp}{2\pi \|\mathbf{x} - \mathbf{x}_j\|^2} \left(1 - \exp\left(-\frac{\|\mathbf{x} - \mathbf{x}_j\|^2}{{\epsilon_j}^2}\right)\right). \tag{15}$$

Note that a similar orthogonal expression can be obtained for the irrotational component, with *source particles* [13].

Let us note that, in the context of fluid flows, other approaches can be considered to reduce the number of state variables describing the model. For instance, it is possible to rely on the global knowledge of the flow in order to construct a reduced representation of it. The flow can then be described by its spectral modes [6] or by spatial basis functions in case of the proper orthogonal decomposition (POD [4]). These methods are widely used for the simulation of fluid flows. For flows exhibiting a repetitive behavior, the POD offers a very efficient representation. Such a decomposition is computed from a series of experimental measures and a singular value decomposition of the autocorrelation function. The reduced dynamical model is then obtained by a Galerkin projection of the most energetic modes on the Navier-Stokes equation. However, such a representation is dedicated to given experimental configuration and cannot be used in a different context. For geophysical applications (meteorology, oceanography, and glaciology), it is difficult to obtain such a basis of realizations of the same phenomenon. These methods are thus not adapted. At the opposite end, the vortex particles allow us to construct a reduced representation of the flow without any a priori knowledge on the flow. Note that, in the same spirit, a wavelet decomposition can also be proposed [18]. However, one advantage of the vortex particles is that the flow dynamics is described by a set of elements, a direct physical interpretation. The approximation is indeed based on the vortices of the flow. Finally, the temporal evolution of the flow can be described on the basis of these elements, from the Navier-Stokes equation. This will be detailed in the next section.

3.2 Vortex Particles Dynamics

The temporal evolution of an incompressible fluid flow (with null divergence) is described in 2D by the Navier-Stokes equation:

$$\frac{\partial \mathbf{w}}{\partial t} + (\mathbf{w} \cdot \nabla)\mathbf{w} = -\frac{1}{\rho}\nabla p + \nu \Delta \mathbf{w}, \tag{16}$$

where p is the pressure, ρ is the fluid density, and ν is the viscosity coefficient of the fluid. The equivalent velocity-vorticity formulation writes

$$\frac{\partial \xi}{\partial t} + (\mathbf{w} \cdot \nabla)\xi = \nu \triangle \xi. \tag{17}$$

In this last formulation, the evolution of the flow is described through the variation of the vorticity, without pressure term. The vorticity is transported by the velocity $\mathbf{w}$ and diffuses according to the viscosity coefficient. This equation can be solved numerically in two distinct steps: the transport and the diffusion steps [7]. The transportation of the vorticity without the diffusion effects is first described by

$$\frac{\partial \xi}{\partial t} + (\mathbf{w} \cdot \nabla)\xi = 0, \tag{18}$$

then the vorticity diffusion (related to the viscosity of the fluid) is described by the heat equation

$$\frac{\partial \xi}{\partial t} = \nu \Delta \xi. \tag{19}$$

3.2.1 Vorticity Transportation

This step is implicitly solved by the Lagrangian nature of the vortex particles. Indeed, the center $\mathbf{x}_l$ of each vortex particle is simply moved by its own velocity $\mathbf{w}(\mathbf{x}_l)$. The displacement of one center $\mathbf{x}_l$ is described by

$$\frac{d\mathbf{x}_l}{dt} = \mathbf{w}(\mathbf{x}_l), \tag{20}$$

where $\mathbf{w}(\mathbf{x}_l)$ is evaluated from all of the other positions following (14):

$$\mathbf{w}(\mathbf{x}_l) = \sum_{j=1}^{q} \gamma_j K_{\epsilon_j}(\mathbf{x}_l - \mathbf{x}_j). \tag{21}$$

In practice, a Gaussian smoothing function is used to compute the kernel K_{ϵ_j}, as written in (15).

We recall that, when the null border conditions for the velocity field cannot be imposed, it is necessary to take the global transportation component (denoted $\mathbf{w}_{tra}$) into account. This component is supposed to be known and can be added to the displacement (21):

$$\mathbf{w}(\mathbf{x}_l) = \sum_{j=1}^{q} \gamma_j K_{\epsilon_j}(\mathbf{x}_l - \mathbf{x}_j) + \mathbf{w}_{tra}(\mathbf{x}_l). \tag{22}$$

3.2.2 Vorticity Diffusion

The diffusion part can be solved by Chorin's *random walk method* [7]. This method is stochastic and relies on the relation between diffusion and Brownian motion. There is indeed a correspondence between the distribution of particles

undergoing a random walk and the solution of the heat equation [9]. The method then consists of applying a Gaussian perturbation to each vortex particle's center. For a time step Δt, the perturbation has zero mean and variance $2\nu\Delta t$. This random displacement is added to the transportation (22).

Note that the diffusion can be simulated by other deterministic methods [12]. However, one advantage of the stochastic approach is that it allows a complete probabilistic interpretation of the 2D incompressible Navier-Stokes equation. In fact, the vorticity-velocity formulation of the Navier-Stokes equation belongs to the class of MacKean-Vlasov equations. It has then a rigorous interpretation in terms of stochastic interacting particles systems [5], [26], [27].

3.2.3 Interacting Particles System

The evolution of the q vortex particles is finally described by the following system:

$$d\mathbf{x}_{l,t} = \sum_{j=1}^{q} \gamma_j K_{\epsilon_j}(\mathbf{x}_{l,t} - \mathbf{x}_{j,t})dt + \sqrt{2\nu}d\mathbf{B}_{l,t}, \quad 1 \leq l \leq q, \quad (23)$$

where $\mathbf{B}_{l,t}$ is a Brownian motion of dimension 2. The system can be rewritten in a compact form, defining $\mathbf{x} = (\mathbf{x}_1, \ldots, \mathbf{x}_q)^T$ and $\mathbf{w}(\mathbf{x}) = (\mathbf{w}(\mathbf{x}_1), \ldots, \mathbf{w}(\mathbf{x}_q))^T$:

$$d\mathbf{x}_t = \mathbf{w}(\mathbf{x}_t)dt + \sqrt{2\nu}d\mathbf{B}_t, \quad (24)$$

where $\mathbf{B}_t$ is a standard Brownian motion of dimension $2q$ with independent components. Note that, in this model, contrary to the general model defined in (1), the diffusion part does not depend on the state $\mathbf{x}_t$ but is only related to the viscosity ν of the fluid.

3.3 State Model for the Filtering Approach

In our filtering model, the state vector $\mathbf{x} = (\mathbf{x}_1, \ldots, \mathbf{x}_q)^T$ is composed of the q centers of vortex particles used to represent the flow. We also recall that the random part of the model (24) expresses the vorticity diffusion. This describes a physical phenomenon but does not include the model uncertainties. These uncertainties may come from various sources: 1) nonadequacy of the 2D model to the image sequence (because we observe 3D phenomena through apparent velocities in the image plane), 2) error in the approximation of the vorticity by a weak number of vortex particles (smoothing of some scales), and 3) bad knowledge of model parameters (strengths and influence domains of vortex particles). In order to include these noise factors into the filtering model, we add an artificial random term η to the state model:

$$d\mathbf{x}_t = \mathbf{w}(\mathbf{x}_t)dt + \sigma_s d\mathbf{B}_t, \quad \text{where} \quad \sigma_s = \sqrt{2\nu} + \eta. \quad (25)$$

3.4 Measurement Model

We recall first that the dense velocity field $\mathbf{w}_t$ can be reconstructed at each time t from the knowledge of the vector $\mathbf{x}_t = (\mathbf{x}_{1,t}, \ldots, \mathbf{x}_{q,t})^T$ and the model parameters. The displacement is given by

$$\mathbf{w}_t(\mathbf{x}) = \sum_{j=1}^{q} \gamma_j K_{\epsilon_j}(\mathbf{x} - \mathbf{x}_{j,t}) \quad \forall \mathbf{x} \in \Omega. \quad (26)$$

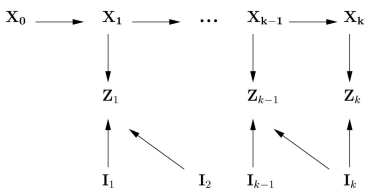

Fig. 1. Dependence graph of the filtering model.

A region R_j is fixed around each center $\mathbf{x}_j$, corresponding to the influence domain of the basis function and characterized by the parameter ϵ_j. Denoting $R = \cup_{j=1}^{q} R_j$, the observation vector is then defined at time t_k by

$$\mathbf{z}_{t_k} = (I_{t_k}(\mathbf{x}))_{\mathbf{x}\in R}, \quad (27)$$

where $I_{t_k}(\mathbf{x})$ is the intensity of the point $\mathbf{x}$ in the image observed at time t_k. The measurement model is based on a brightness consistency assumption

$$I_{t_k}(\mathbf{x}) = I_{t_{k+1}}(\mathbf{x} + \mathbf{w}_{t_k}(\mathbf{x})) + u_{t_k}, \quad (28)$$

defined up to a Gaussian noise $u_{t_k} \sim \mathcal{N}(0, \sigma_m^2)$. The parameter σ_m controls the uncertainty in the measurement model. This term traduces the uncertainty in the observations if the quality of observed images is bad for instance. Besides, this uncertainty term allows dealing with an eventual nonvalidity of the brightness consistency assumption. Let us note that this general brightness consistency model can be adapted to specific situations [2], [20], [22], [21].

Assuming that $I_{t_k}(\mathbf{x})$ and $I_{t_k}(\mathbf{x}')$ are independent conditionally to $\mathbf{x}_{t_k}$ $\forall(\mathbf{x}, \mathbf{x}') \in R$, the likelihood of the vector of observations $\mathbf{z}_{t_k}$ reads

$$p(\mathbf{z}_{t_k}|\mathbf{x}_{t_k}) = \prod_{\mathbf{x}\in R} p(I_{t_k}(\mathbf{x})|\mathbf{x}_{t_k}) \quad (29)$$

and, consequently,

$$p(\mathbf{z}_{t_k}|\mathbf{x}_{t_k}) \propto \exp\left(-\int_R \frac{\left(I_{t_k}(\mathbf{x}) - I_{t_{k+1}}(\mathbf{x} + \mathbf{w}_{t_k}(\mathbf{x}))\right)^2}{2\sigma_m^2} d\mathbf{x}\right). \quad (30)$$

Note that the construction of the likelihood at time t_k relies on the assumption that the image $I_{t_{k+1}}$ is available. The dependence graph of our filtering model is then described by Fig. 1.

3.5 Filtering Scheme for Velocity Fields Tracking

The complete filtering model is finally defined by the state model (25) and the likelihood (30)

$$\begin{cases} d\mathbf{x}_t = \mathbf{w}(\mathbf{x}_t)dt + \sigma_s d\mathbf{B}_t, \\ p(\mathbf{z}_{t_k}|\mathbf{x}_{t_k}). \end{cases} \quad (31)$$

As both the evolution model and the measurement model are nonlinear, a nonlinear filtering technique must be used to solve the filtering problem. The particle filter for a continuous-discrete model, as presented in Section 2.3, is adapted to such a highly nonlinear problem. The overall velocity fields tracking method is finally composed of the following steps:

- $\mathbf{t_k = t_0}$: Initialization of the state vector $\mathbf{x}_{t_0} = (\mathbf{x}_{1,t_0}, \ldots, \mathbf{x}_{q,t_0})^T$ composed of q vortex particles positions and their associated strength and influence parameters $\{\gamma_j, \epsilon_j\}_{j=1:q}$. Note that the influence parameters are initialized so that vortex particles overlap. The initial vorticity distribution is then estimated from the first pair of images. The corresponding parameters estimation problem is constructed from the representation (15), incorporated within a spatiotemporal variation model of the luminance function. This estimation method has been described in previous papers [15], [13].
- $\mathbf{t_k = t_1, t_2, \ldots}$:
  - **Prediction of vortex particles trajectories:** Simulation of N trajectories $\{\mathbf{x}_t^{(i)} : t_{k-1} < t \leq t_k\}_{i=1:\mathrm{N}}$ from the initial conditions $\{\mathbf{x}_{t_{k-1}}^{(i)}\}_{i=1:\mathrm{N}}$ with the Euler scheme:

$$\begin{aligned} &\mathbf{x}_{t+\Delta t}^{(i)} = \mathbf{x}_t^{(i)} + \mathbf{w}\left(\mathbf{x}_t^{(i)}\right)\Delta t + \sigma_s\sqrt{\Delta t}\eta_t^{(i)}, \\ &\text{where} \quad \eta_t^{(i)} \sim \mathcal{N}(0, \mathbb{I}_{2q}). \end{aligned} \tag{32}$$

  - **Correction and normalization of trajectories weights:**

$$\begin{aligned} &w_{t_k}^{(i)} \propto w_{t_{k-1}}^{(i)} p\left(\mathbf{z}_{t_k}|\mathbf{x}_{t_k}^{(i)}\right) \quad \text{and} \\ &\widetilde{w}_{t_k}^{(i)} = \frac{w_{t_k}^{(i)}}{\sum_{j=1}^{\mathrm{N}} w_{t_k}^{(j)}} \quad i = 1 : \mathrm{N}. \end{aligned} \tag{33}$$

  - **Estimation:**
    * Estimated filtering distribution:

$$\hat{p}(\mathbf{x}_{t_k}|\mathbf{z}_{t_1:t_k}) = \sum_{i=1}^{\mathrm{N}} \widetilde{w}_{t_k}^{(i)} \delta_{\mathbf{x}_{t_k}^{(i)}}(\mathbf{x}_{t_k}). \tag{34}$$

    * Estimated state:

$$\hat{\mathbf{x}}_{t_k} = (\hat{\mathbf{x}}_{1,t_k}, \ldots, \hat{\mathbf{x}}_{q,t_k})^T = \sum_{i=1}^{\mathrm{N}} \widetilde{w}_{t_k}^{(i)} \mathbf{x}_{t_k}^{(i)}. \tag{35}$$

    * Estimated velocity field:

$$\hat{\mathbf{w}}_{t_k}(\mathbf{x}) = \sum_{j=1}^{q} \gamma_j K_{\epsilon_j}(\mathbf{x} - \hat{\mathbf{x}}_{j,t_k}) \quad \forall \mathbf{x} \in \Omega. \tag{36}$$

Note that the filtering distribution $\hat{p}(\mathbf{x}_{t_k}|\mathbf{z}_{t_1:t_k})$ is estimated at observations times t_k only. However, it can be defined between two measurement times t_{k-1} and t_k by its predicted form

$$p(\mathbf{x}_t|\mathbf{z}_{t_1:t_{k-1}}) \quad \text{for} \quad t_{k-1} < t < t_k. \tag{37}$$

This distribution can be approximated on the set of trajectories $\{\mathbf{x}_t^{(i)}\}_{i=1:\mathrm{N}}$, simulated according to the scheme (32) and weighted by the weights evaluated at t_{k-1}:

$$\hat{p}(\mathbf{x}_t|\mathbf{z}_{t_1:t_{k-1}}) = \sum_{i=1}^{\mathrm{N}} \widetilde{w}_{t_{k-1}}^{(i)} \delta_{\mathbf{x}_t^{(i)}}(\mathbf{x}_t), \tag{38}$$

leading to

$$\hat{\mathbf{x}}_t = (\hat{\mathbf{x}}_{1,t}, \ldots, \hat{\mathbf{x}}_{q,t})^T = \sum_{i=1}^{\mathrm{N}} \widetilde{w}_{t_{k-1}}^{(i)} \mathbf{x}_t^{(i)}. \tag{39}$$

The velocity fields can then be estimated for all t between two instants of measurements:

$$\hat{\mathbf{w}}_t(\mathbf{x}) = \sum_{j=1}^{q} \gamma_j K_{\epsilon_j}(\mathbf{x} - \hat{\mathbf{x}}_{j,t}) \quad \forall \mathbf{x} \in \Omega. \tag{40}$$

4 Dimensional Reduction of the Filtering Problem

When the dimension of the state space is high, the implementation of filtering techniques is problematic. The difficulty is related to the handling of estimated error covariance matrices for the Kalman filter and its extensions and to the number of sampled trajectories for Monte-Carlo filtering techniques. A first way to reduce the size of the problem is to construct a reduced representation of the state. The vortex particle decomposition is such a reduced size representation for the dense velocity fields tracking problem. However, when the phenomenon is too complex, the size of this representation remains high. A second approach consists of relying on the analysis of stable and unstable directions of a dynamical system. This idea has been used for the Kalman filtering techniques in order to approximate the estimated covariance matrix by a reduced rank one [28], [32]. For the continuous-discrete particle filter, a method has been proposed by Chorin and Krause [8]. The idea is to concentrate the sampling effort over unstable directions of the dynamics, defined adaptively along the sequential estimation process.

Following Chorin and Krause's paper, we present in this section a way to characterize the stable and unstable directions of a dynamical system. The reduced version of the continuous-discrete particle filter is then applied to our model.

4.1 Stable and Unstable Directions of a Dynamical System

4.1.1 General Case

We consider the following differential equation, describing the evolution of a system without noise:

$$\frac{d\mathbf{x}_t}{dt} = f(\mathbf{x}_t). \tag{41}$$

Let $[t_{j-1}, t_j]$ be a time interval of finite length. Let $\mathbf{x}_{t_{j-1}}$ be the state vector of the system at time t_{j-1} and $\mathbf{x}_{t_{j-1}} + \delta\mathbf{x}_{t_{j-1}}$ a small perturbation of $\mathbf{x}_{t_{j-1}}$. The temporal evolution of $\delta\mathbf{x}(t)$ can be approximated by the linear equation

$$\frac{d\delta\mathbf{x}_t}{dt} = J(t)\delta\mathbf{x}_t, \tag{42}$$

where $J(t) = \frac{\partial f}{\partial \mathbf{x}}(\mathbf{x}(t))$ is the Jacobian matrix of f, evaluated at $\mathbf{x}(t)$. The solution of this linear system is given at time t_j by

$$\delta\mathbf{x}(t_j) = M_{t_{j-1},t_j}\delta\mathbf{x}(t_{j-1}), \tag{43}$$

where M_{t_{j-1},t_j} is called the resolvant matrix of the system, defined through matrix exponential as

$$M_{t_{j-1},t_j} = \exp\left(\int_{t_{j-1}}^{t_j} J(s)ds\right). \tag{44}$$

Observing that

$$< \delta\mathbf{x}(t_j), \delta\mathbf{x}(t_j) > = < M_{t_{j-1},t_j}\delta\mathbf{x}(t_{j-1}), M_{t_{j-1},t_j}\delta\mathbf{x}(t_{j-1}) > \tag{45}$$

$$= < \delta\mathbf{x}(t_{j-1}), M^T_{t_{j-1},t_j}M_{t_{j-1},t_j}\delta\mathbf{x}(t_{j-1}) >, \tag{46}$$

where $<,>$ denotes the euclidean scalar product, it follows that the directions of the highest growth of the perturbation over an interval $[t_{j-1}, t_j]$ can be characterized by the eigenvectors of the matrix $M^T_{t_{j-1},t_j}M_{t_{j-1},t_j}$. The eigenvectors associated to the eigenvalues greater than 1 correspond to the *unstable* directions, while the remaining eigenvectors correspond to the *stable* ones.

4.1.2 Vortex Particles Model

The state evolution model of the vortex particles (25) without the noise component is given by

$$\frac{d\mathbf{x}_t}{dt} = \mathbf{w}(\mathbf{x}_t), \tag{47}$$

where we recall that $\mathbf{x} = (\mathbf{x}_1, \ldots, \mathbf{x}_q)^T$ and $\mathbf{w}(\mathbf{x}) = (\mathbf{w}(\mathbf{x}_1), \ldots, \mathbf{w}(\mathbf{x}_q))^T$. The Jacobian matrix $J(t) = \frac{\partial \mathbf{w}}{\partial \mathbf{x}}(\mathbf{x}(t))$ of size $(2q, 2q)$ is first constructed from the velocity expression (15). The resolvant matrix is then computed from (44).

4.2 Reduced Continuous-Discrete Particle Filter

Let us first note that if the time interval $[t_{k-1}, t_k]$ between two observations is long, the interval is first divided as follows: $[t_{k-1}, t_k] = \cup_j [t_{j-1}, t_j]$. The stable and unstable directions are then computed with more precision over successive subintervals. Over a given subinterval $[t_{j-1}, t_j]$, the stable and unstable directions of the system (47) are specified from a deterministic test trajectory denoted $\widetilde{\mathbf{x}}(t)$. This trajectory is obtained by propagation of the estimated state $\hat{\mathbf{x}}_{t_{j-1}}$ from time t_{j-1} to time t_j, integrating the model (47) with a standard Euler scheme of time step Δt:

$$\mathbf{x}_{t+\Delta t} = \mathbf{x}_t + \mathbf{w}(\mathbf{x}_t)\Delta t. \tag{48}$$

The matrix M_{t_{j-1},t_j} is evaluated along the test trajectory using (44). We denote by Q the matrix composed of the eigenvectors of $M^T_{t_{j-1},t_j}M_{t_{j-1},t_j}$. The change of variables $\mathbf{y} = Q\mathbf{x}$ leads to the following reformulation of our state evolution model (25):

$$d\mathbf{y}_t = Q\mathbf{w}(Q^T\mathbf{y}_t)dt + Q\Sigma_s d\mathbf{B}_t, \quad \text{where} \quad \Sigma_s = \sigma_s \mathbb{I}_{2q}. \tag{49}$$

The continuous-discrete particle filter is then modified as follows:

- $\mathbf{t_k} = \mathbf{t_1}, \mathbf{t_2}, \ldots$:
  - **Adaptive prediction of trajectories**:
    Over all subintervals $[t_{j-1}, t_j]$ such that $\cup_j [t_{j-1}, t_j] = [t_{k-1}, t_k]$:
    * Characterization of the m unstable and $2q - m$ stable components of the system (see Section 4.1).
    * Simulation of N trajectories $\{\mathbf{y}_t^{(i)} : t_{j-1} < t \leq t_j\}_{i=1:\mathrm{N}}$ from the initial conditions $\{\mathbf{y}_{t_{j-1}}^{(i)}\}_{i=1:\mathrm{N}}$, handling differently the unstable and stable components.
      - Unstable components: Simulated from the model (49).
      - Stable components: Replaced by the corresponding components of the test trajectory $\widetilde{\mathbf{y}} = Q\widetilde{\mathbf{x}}$.
  - **Correction and estimation:** After change of variable $\mathbf{x} = Q^T\mathbf{y}$, use of (33) to (36).

The dimensional reduction acts over the prediction step of the filtering algorithm. For each trajectory, the m unstable components are randomly sampled, while the $2q - m$ stable components are fixed to the deterministic test trajectory components. The sampling problem associated to the prediction step is then reduced to a state space of size m.

5 Experimental Validation

This section shows a set of experiments designed to validate the tracking method we propose. The nonlinear filtering technique is first tested on synthetic image sequences. The first sequence has been synthesized from a reduced model of vortex particles. The second sequence comes from a numerical simulation of a bidimensional turbulent flow. Results on real-world sequences are then presented. The first sequence is related to experimental fluid mechanics, whereas the second one is an infrared meteorological sequence.

5.1 Synthetic Image Sequence of Vortex Particles

We present in this section the tracking results on a synthetic image sequence simulated from a reduced model of vortex particles. The model has been constructed from five vortex particles. Their initial positions $\{\mathbf{x}_{j,t_0}\}_{j=1:5}$ and associated parameters $\{\gamma_j, \epsilon_j\}_{j=1:5}$ have been fixed. The state of the model is defined as the set of the positions of the five particles, and its evolution is characterized by the model (25). Vortex particle trajectories can be simulated from the state model, with a discretization scheme of Euler type. We show, in Fig. 2, an example of two realizations, obtained from the same initial conditions. The temporal evolution of each coordinate of the state vector can be seen in Fig. 2 for 100 time steps. It can be noticed that the trajectories simulated from the stochastic differential equation can differ a lot.

In order to test the tracking method, we have first selected one of the trajectories simulated from the model as a reference. The realization we have chosen is the one plotted in black in Fig. 2. From this reference trajectory, a sequence of velocity fields has been obtained using expression (15). A sequence of synthetic images has then

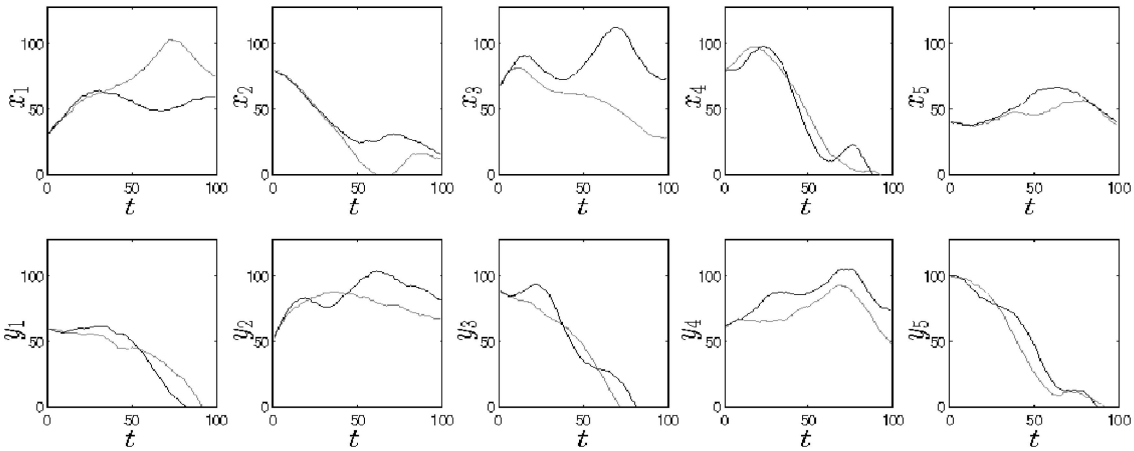

Fig. 2. *Example of two realizations obtained by simulation of the model constructed from five vortex particles.* Temporal trajectories of the 10 coordinates of the five vortex particles (the realization corresponding to the ground truth is plotted in black).

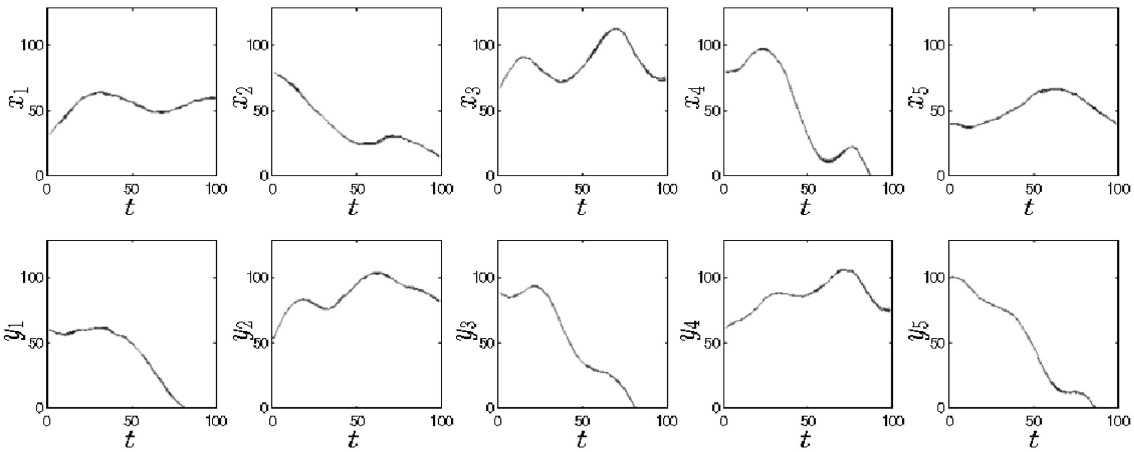

Fig. 3. *Tracking result obtained with the nonlinear filtering method we propose averaged over 50 filterings.* Temporal trajectories of the 10 coordinates of the five vortex particles (the ground truth is plotted in black, the mean result of the tracking in dark gray, and the dispersion of the estimations around their means in light gray).

been constructed by warping. A pair $(I_{t_k}, I_{t_{k+1}})$ of synthetic images is then available at each observation time t_k. The motion described by this pair corresponds to the displacement at time t_k of the ground truth. The images we have used to create the synthetic sequence correspond to images of small particles transported by the flow, similar to the ones used by Particle Image Velocimetry (PIV) techniques (see Fig. 6 for an illustration of such images).

We have tested the tracking method on this synthetic image sequence, with $\mathrm{N} = 500$ trajectories. The result is presented in Fig. 3. In order to evaluate the robustness of the particle filtering method against its stochasticity, we have represented a mean result over 50 filterings and the dispersion around this result. The results show that the method is able to recover the test trajectory. The estimated trajectories of the five vortex particles coincide with the trajectories associated to the ground truth (see Fig. 3). The dispersion around the estimation of each coordinate of the state vector is very weak, highlighting the robustness of the tracking method.

In order to demonstrate the interest of a continuous modeling of our filtering problem, the tracking method has been tested on the same image sequence, but for a state space model in discrete time. In that case, the discretization step of the evolution model corresponds to the time step between two images. The evolution equation then writes as follows:

$$\mathbf{x}_{t_{k+1}} = \mathbf{x}_{t_k} + \mathbf{w}(\mathbf{x}_{t_k}) + \mathbf{v}_{t_k}, \tag{50}$$

where $\mathbf{v}_{t_k}$ is a Gaussian noise. The corresponding filtering result is presented in Fig. 4. The result corresponds to a mean over 50 filterings. We can notice that the estimated trajectories of the vortices do not recover the true trajectories. Moreover, Fig. 4 shows that the dispersion around the estimates is quite high. This experiment highlights the importance of a continuous modeling in case of a vorticity-velocity dynamics.

The last experiment on this synthetic sequence concerns the dimensional reduction presented in Section 4. The tracking result obtained with the reduced particle filter has been compared to the result we have presented in Fig. 3, for the same number of trajectories $(\mathrm{N} = 500)$. The comparison has been done in terms of mean absolute vorticity estimation error at each time. The result is presented in Fig. 5. The number m of unstable components is equal to 5 so that the reduction we have obtained is of factor 2.

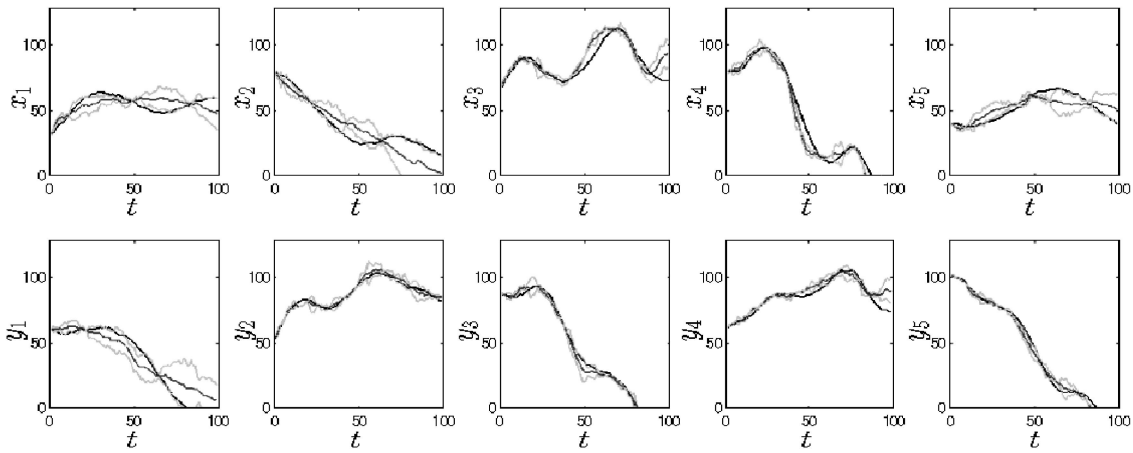

Fig. 4. *Tracking result obtained with a discrete model, averaged over 50 filterings.* Temporal trajectories of the 10 coordinates of the five vortex particles (the ground truth is plotted in black, the mean result of the tracking in dark gray, and the dispersion of the estimations around their means in light gray).

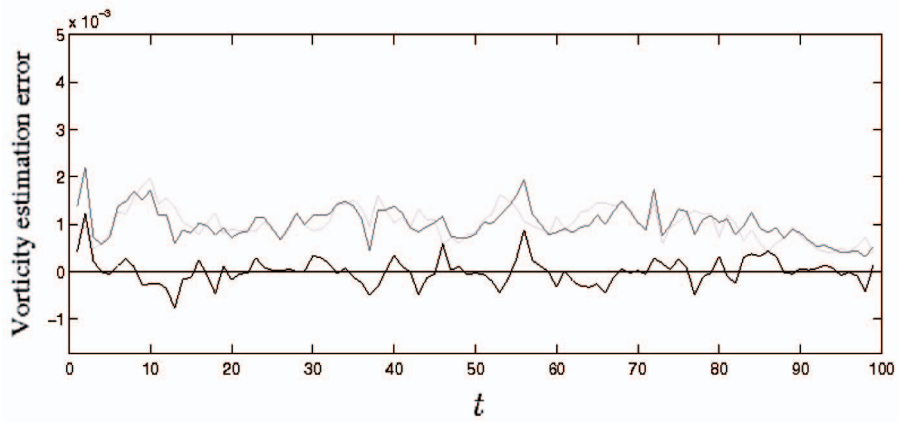

Fig. 5. *Comparison of the tracking results by filtering with and without dimensional reduction.* The mean vorticity estimation error associated to the dimensional reduction is plotted in dark gray and the error associated to the result presented in Fig. 3 is plotted in light gray. The black curve represents the difference.

Surprisingly, this factor 2 is repeated over the whole sequence. For a reduction of factor 2, note that the gain in computational cost was negligible due to the computational cost associated with the determination of the eigenvalues. However, it can be observed in Fig. 5 that the tracking results obtained with or without dimensional reduction are close. This shows that the random sampling can be done in a space of reduced size without loss of quality if this reduced space is defined properly.

5.2 Synthetic Image Sequence of 2D Turbulence

We present a second synthetic example showing the temporal evolution of a 2D turbulent flow. This image sequence of 100 frames has been obtained by simulation of the 2D incompressible Navier-Stokes equation with a DNS method.[1] The sequence is partly reproduced in Fig. 6.

A sequence of vorticity maps corresponding to the simulation of the flow is represented in Fig. 7. The filtering model has been initialized on the first pair of images with the estimation method proposed in [13]. The state vector is composed of 100 vortex particles. It is then of size 200, leading to a more difficult problem than the previous example. However, as we are limited in practice by the computational resources, we have restricted the number of sampled trajectories to $\mathrm{N} = 1{,}000$. Fig. 7 displays the temporal evolution of the vorticity maps corresponding to the numerical simulation and the evolution of the maps estimated by the tracking method. The estimated initial vorticity distribution can be compared to the true initial vorticity in Fig. 7, at time $t_k = 0$. We can observe that the reduced model allows to recover the large scales of vorticity, while the smaller scales of the flow tend to be smoothed. For that reason, the filtering method is not able to track the fine structures of vorticity. However, we can notice that the main vortices of the flow are tracked correctly. For instance, the temporal evolution of the vortex located in the bottom right corner of the image at time $t_k = 0$ can be observed. Its trajectory is well tracked over the whole sequence. The corresponding motion fields can be compared in Fig. 8.

A quantitative analysis of the tracking result is presented in Fig. 9. This figure displays the temporal evolution of the absolute vorticity error between the true vorticity and the estimated vorticity, averaged over the image. This error can

1. The image sequence has been provided by the CEMAGREF Rennes within the framework of the European FLUID project "Fluid Image Analysis and Description" http://fluid.irisa.fr.

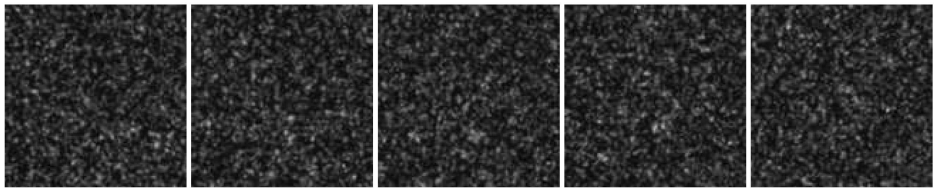

Fig. 6. Image sequence obtained by Direct Numerical Simulation of the 2D incompressible Navier-Stokes equation.

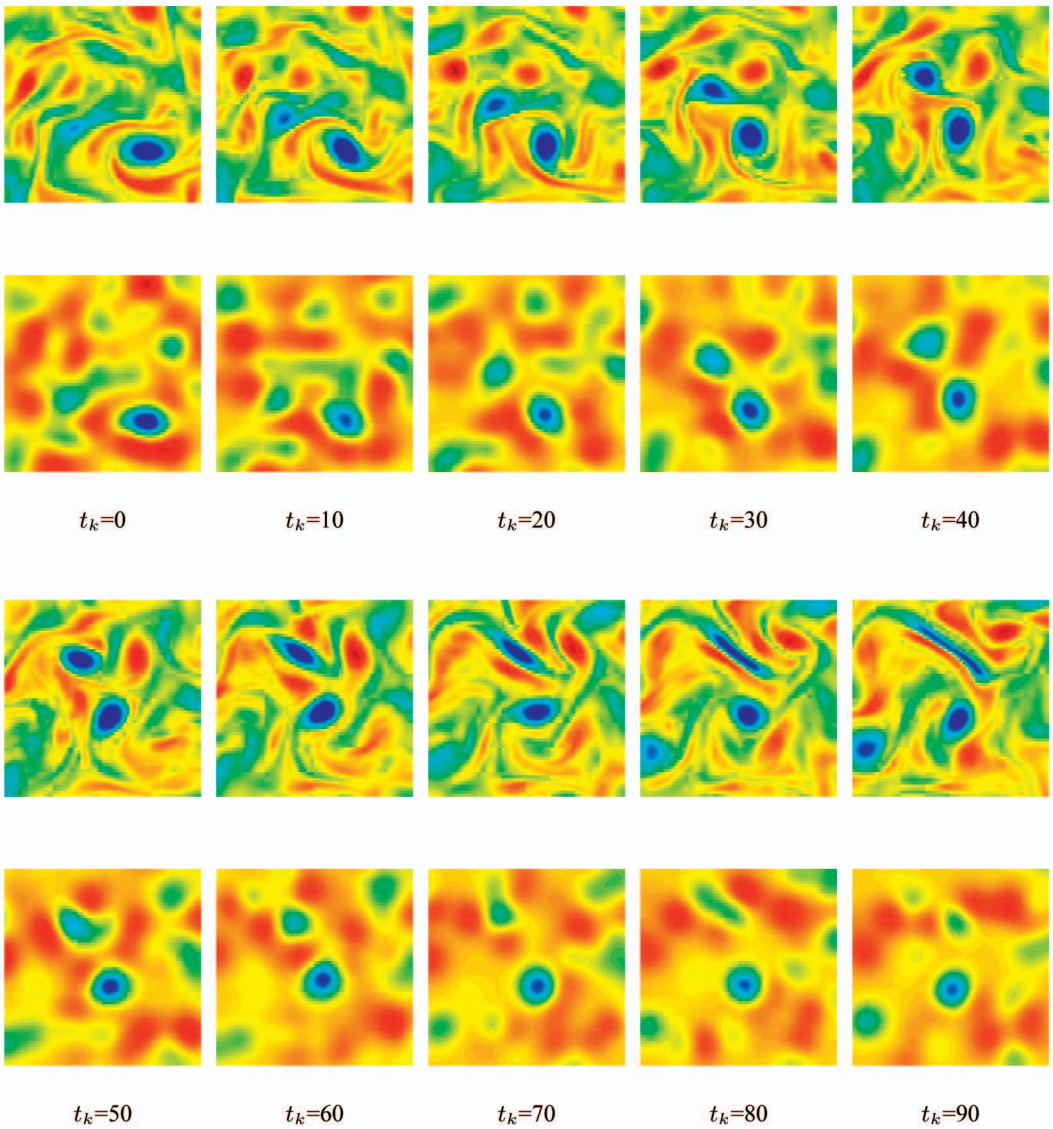

Fig. 7. *Result for 2D turbulence tracking: comparison of the vorticity maps.* The ground truth is presented in the first line and the tracking result in the second line.

be compared to the temporal evolution of the error obtained with a simple propagation in time of the model. Let us note that the mean absolute error of the tracking method is not negligible in comparison with the mean absolute vorticity over this sequence. However, we can note that the tracking leads to a significant improvement in comparison with a simple prediction of the model.

5.3 Experimental Fluid Mechanics Application

The tracking method has been tested on a real image sequence coming from an application in experimental fluid mechanics. The sequence shows the evolution of a vortex generated at the tip of an airplane wing.[2] The sequence, composed of 160 frames, is partly reproduced in Fig. 10.

The initialization of the model has been obtained from the first pair of images of the sequence. The initial vorticity distribution is described by a set of 15 vortex particles. This vorticity map and the corresponding displacement field can be seen in Fig. 11 for $t_k = 0$. Fig. 11 illustrates the results

2. The sequence has been provided by the Office National d'Études et de Recherches Aérospatiales (ONERA).

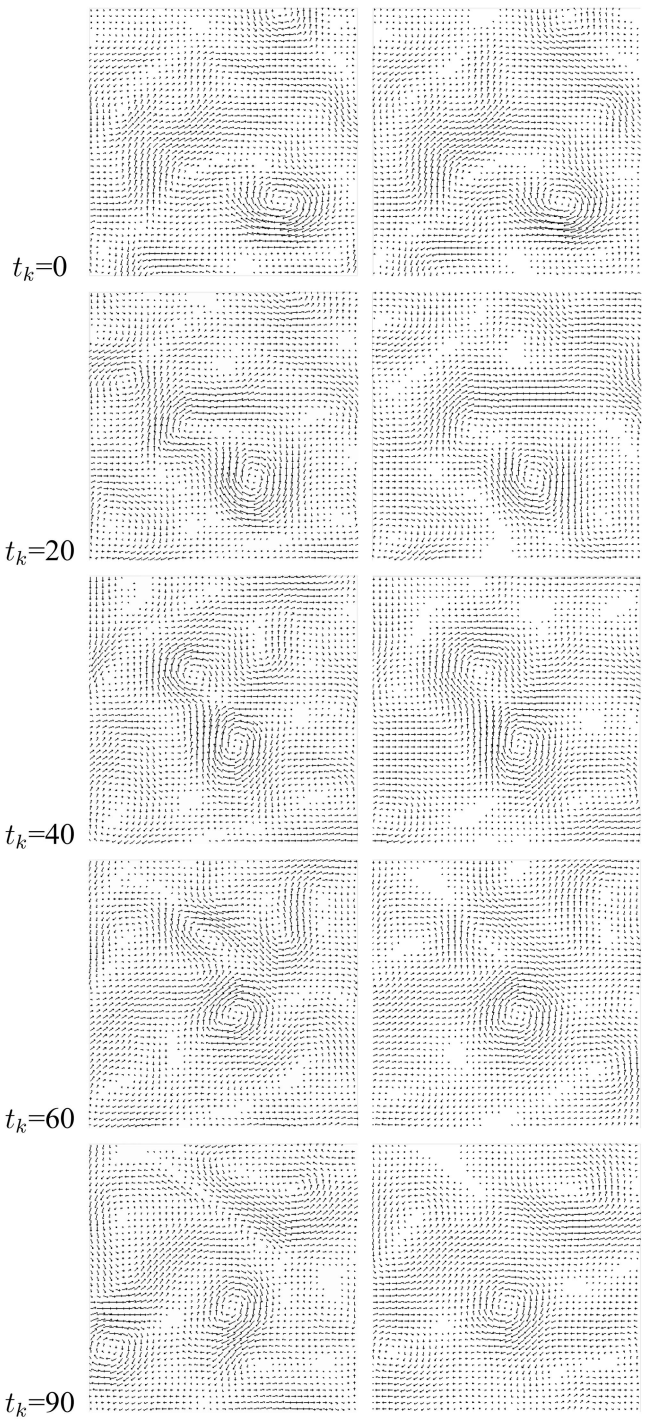

Fig. 8. Result for 2D turbulence tracking: Comparison of the displacement fields. The ground truth is presented in the first column and the tracking result in the second column.

obtained by a simple propagation of the model. We can observe that a simple simulation of the dynamical model does not enable to track the vortex over the whole sequence. Indeed, from time $t_k = 20$, the shape of the vortex is not well reconstructed. The predicted displacement fields deviate significantly from the center of the vortex. Later in the sequence, the predicted displacement fields present deformations that do not correspond to the observed phenomenon.

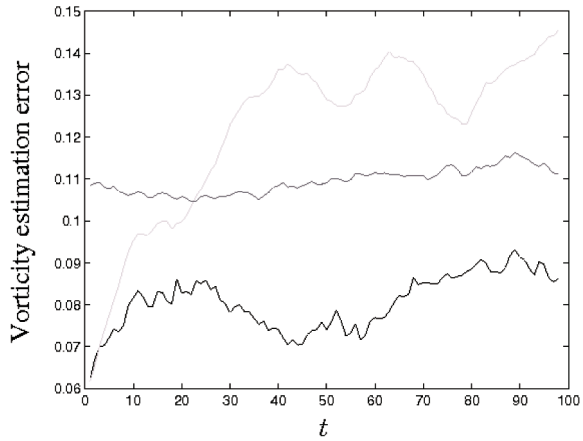

Fig. 9. *Temporal evolution of the absolute vorticity error, averaged over the image domain.* The estimation error caused by a simple propagation of the evolution model is plotted in light gray and the estimation error of the tracking method is plotted in black. The mean absolute vorticity corresponding to the ground truth is plotted in dark gray.

In the final part of the sequence, the trajectory of the vortex is completely lost.

Fig. 12 shows the solution obtained by the tracking method, for $\mathrm{N} = 1{,}000$ trajectories in the filtering algorithm. The motion of the vortex is well reconstructed at each time and its trajectory is well tracked until the end of the sequence. In particular, we can observe that the diffusion of the vortex in the second half of the sequence is well represented by the displacement fields. The deformation of the estimated rotating motion follows the photometric contours of the image. Secondary counter-vortices rotating around the principal vortex are well represented. The evolution of the associated vorticity maps shows a spatial diffusion of the positions of the vortex particles. The diffusion of the vortex is described by the fact that the associated vorticity area becomes less concentrated in space.

For these real examples, the actual displacement fields are not known. However, an indication about the quality of the results can be given by the mean reconstruction error over the image domain, from the estimated displacement fields. This error is defined at each observation time t_k by $|I_{t_{k+1}}(\mathbf{x} + \hat{\mathbf{w}}_{t_k}(\mathbf{x})) - I_{t_k}(\mathbf{x})| \quad \forall \mathbf{x} \in \Omega$. The mean error evolution is represented in Fig. 13. An indication about the quality of the result given by the prediction can be compared to the result of the tracking method we have proposed. The algorithm has been run 20 times in order to test the robustness of the method. The mean result and the dispersion of the estimations around this mean are displayed at each time in the figure. We can observe that the reconstruction error related to the prediction is highly decreased by the introduction of the observations in the filtering model. This remark confirms the qualitative comparison we have done from Figs. 11 and 12.

5.4 Meteorology Application

We present in this section a result obtained on a sequence of images provided by the infrared channel of Meteosat.[3] The

3. The sequence has been provided by the Laboratoire de Météorologie Dynamique (LMD) within the framework of the European FLUID project "Fluid Image Analysis and Description" http://fluid.irisa.fr.

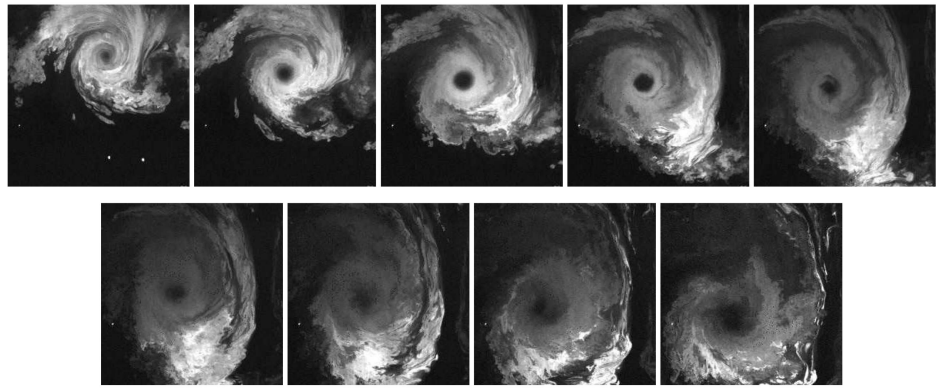

Fig. 10. Image sequence showing the evolution of a vortex generated at the tip of an airplane wing.

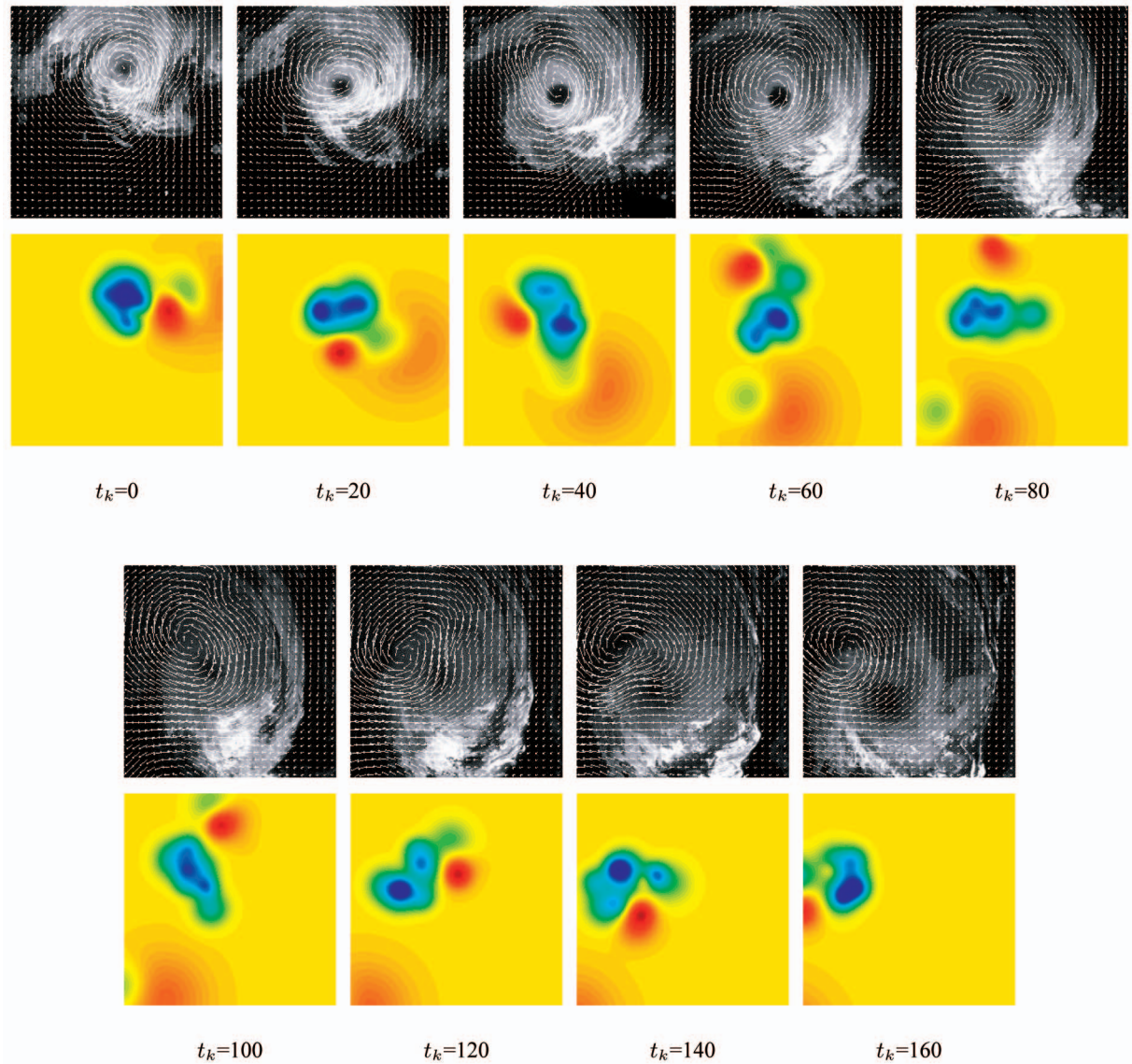

Fig. 11. Vortex tracking result on the ONERA sequence by simple propagation of the evolution model.

sequence displays the trajectory of a cyclone over the Indian Ocean. The sequence is partly represented in Fig. 14.

The tracking result with the filtering method is presented in Fig. 15. The initialization is described by the displacement field and the vorticity distribution estimated at time $t_k = 0$ from the first pair of images, with a set of 15 vortex particles. The rotating motion described by the cyclone is well reconstructed and its trajectory is well tracked until the end of the sequence. The temporal evolution of the mean reconstruction error is plotted in Fig. 16.

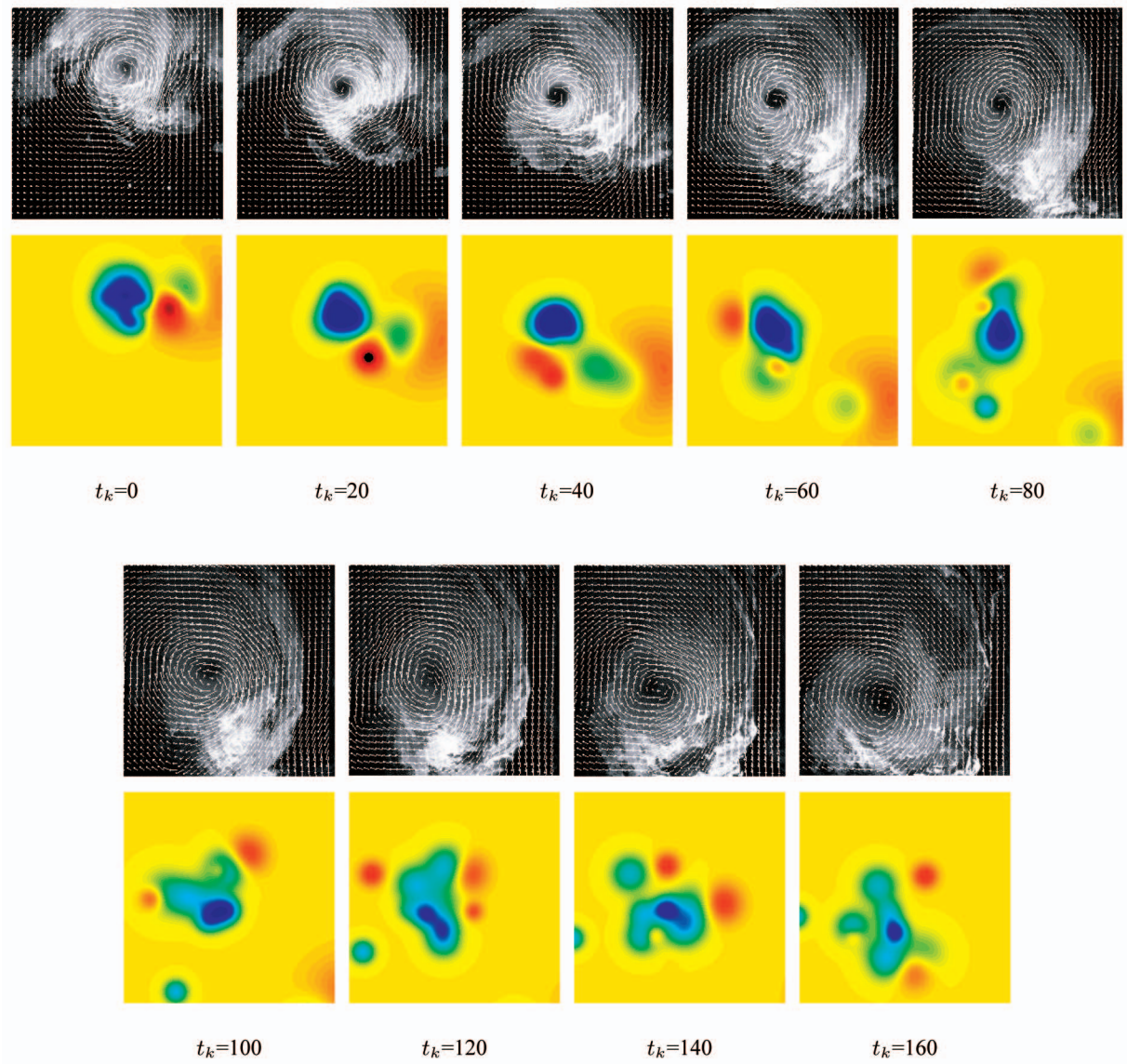

Fig. 12. Vortex tracking result on the ONERA sequence with the proposed method.

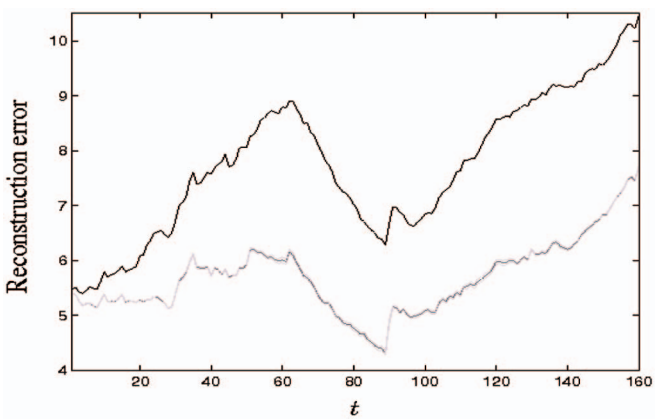

Fig. 13. *Temporal evolution of the mean reconstruction error on the ONERA sequence.* The error associated to a simple prediction of the model is plotted in black, the mean error corresponding to the filtering method is plotted in dark gray and the dispersion around the mean in light gray.

6 Conclusion

In this paper, we have proposed a nonlinear stochastic filter for the tracking of fluid flow velocity fields from image sequences. In order to improve the robustness and the temporal consistency of the successive estimates, a physical knowledge about the fluid evolution law has been introduced into the filtering model. The evolution law of the filtering model is based on the vorticity-velocity form of the Navier-Stokes equation. The discretization of the vorticity over a set of basis functions (called vortex particles) allows us to describe the dynamical model by a stochastic differential equation. This equation is constructed from a reduced number of vortex particles; consequently, it is only an approximation of the Navier-Stokes equation. However, this continuous evolution model brings very useful a priori information about the fluid flow evolution, which is then corrected by the discrete observations extracted from the image sequence. A continuous form of the particle filter algorithm has been applied to solve the

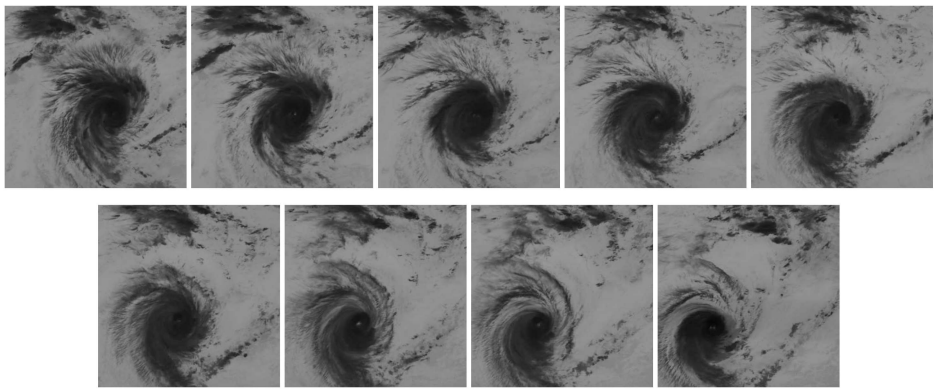

Fig. 14. Image sequence displaying the evolution of a cyclone in the Indian Ocean.

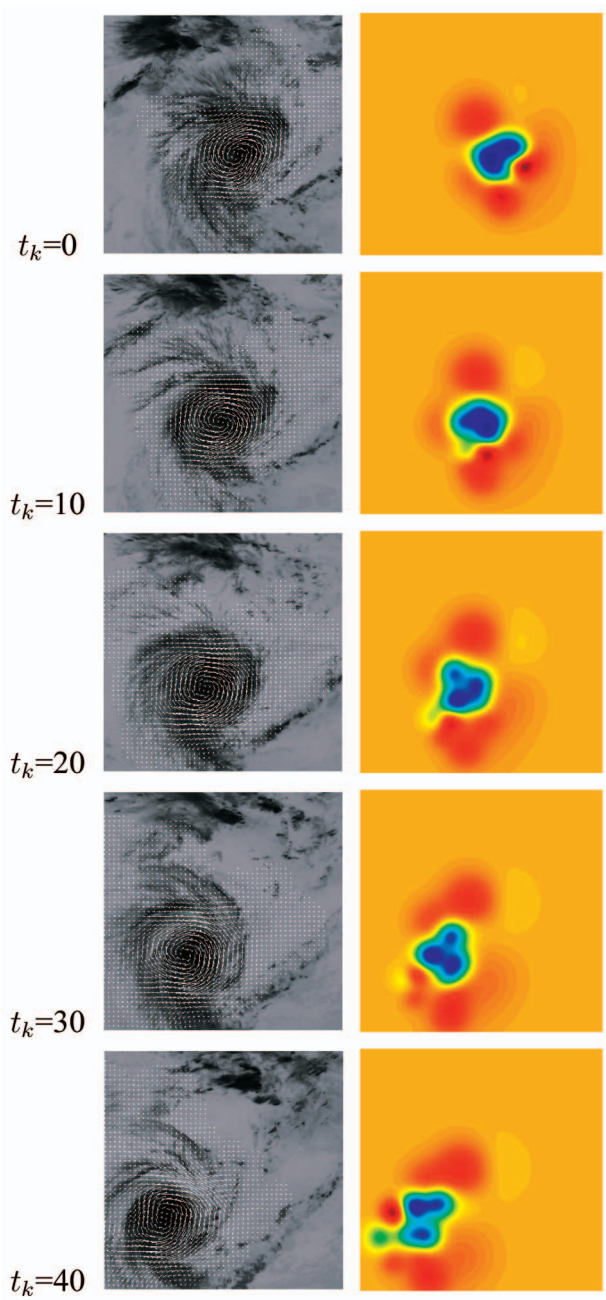

Fig. 15. Cyclone tracking result with the proposed method.

nonlinear filtering problem. Because the particle filter is not adapted to state spaces of high dimension, a dimensional reduction method has been used, based on the study of the instabilities of the system. The results show that the tracking method gives good results on synthetic and real-world sequences, when the flow can be described by a reduced number of vortex particles. For complex flows, results are promising since the evolution of the large-scale components of the flow can be recovered. Finally, let us note that a necessary extension of this work is to focus on the parameter estimation problem in the filtering model. As a matter of fact, the vortex particle parameters (strength and size) are fixed in our model, but a better approach would be to let them evolve in time. The associated filtering problem would then consist of solving the joint estimation of the state and parameters of the model at each time step.

ACKNOWLEDGMENTS

The authors would like to thank ONERA for providing them with the experimental data of wingtip vortices. This work was supported by the European community through the IST Fet open FLUID project (http://fluid.irisa.fr).

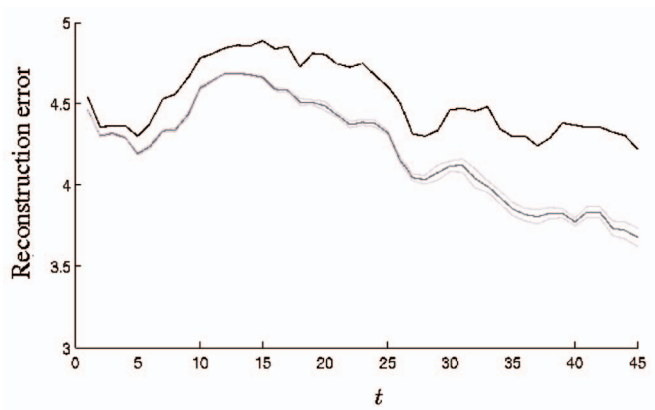

Fig. 16. *Temporal evolution of the mean reconstruction error for the cyclone sequence.* The error associated to a simple prediction of the model is plotted in black, the mean error corresponding to the filtering method is plotted in dark gray, and the dispersion around this mean is plotted in light gray.

REFERENCES

[1] E. Arnaud and E. Mémin, "Partial Linear Gaussian Models for Tracking in Image Sequences Using Sequential Monte Carlo Methods," *Int'l J. Computer Vision,* vol. 74, no. 1, pp. 75-102, 2007.

[2] E. Arnaud, E. Mémin, R. Sosa, and G. Artana, "A Fluid Motion Estimator for Schlieren Imaging Velocimetry," *Proc. European Conf. Comp. Vision,* May 2006.

[3] J. Barron, D. Fleet, and S. Beauchemin, "Performance of Optical Flow Techniques," *Int'l J. Computer Vision,* vol. 12, no. 1, pp. 43-77, 1994.

[4] G. Berkooz, P. Holmes, and J. Lumley, "The Proper Orthogonal Decomposition in the Analysis of Turbulent Flows," *Ann. Rev. Fluid Mechanics,* vol. 25, pp. 539-575, 1993.

[5] M. Bossy, "Some Stochastic Particle Methods for Nonlinear Parabolic PDEs," *Proc. European Series in Applied and Industrial Math.,* vol. 15, pp. 18-57, 2005.

[6] C. Canuto, M. Hussaini, A. Quarteroni, and T. Zang, *Spectral Methods in Fluid Dynamics.* Springer, 1988.

[7] A.J. Chorin, "Numerical Study of Slightly Viscous Flow," *J. Fluid Mechanics,* vol. 57, pp. 785-796, 1973.

[8] A.J. Chorin and P. Krause, "Dimensional Reduction for a Bayesian Filter," *Proc. Nat'l Academy of Sciences USA,* vol. 101, no. 42, 2004.

[9] A.J. Chorin and J.E. Marsden, *A Mathematical Introduction to Fluid Mechanics.* Springer-Verlag, 1993.

[10] T. Corpetti, E. Mémin, and P. Pérez, "Dense Estimation of Fluid Flows," *IEEE Trans. Pattern Analysis and Machine Intelligence,* vol. 24, no. 3, pp. 365-380, Mar. 2002.

[11] T. Corpetti, E. Mémin, and P. Pérez, "Extraction of Singular Points from Dense Motion Fields: An Analytic Approach," *J. Math. Imaging and Vision,* vol. 19, no. 3, pp. 175-198, 2003.

[12] G.-H. Cottet and P. Koumoutsakos, *Vortex Methods: Theory and Practice.* Cambridge Univ. Press, 2000.

[13] A. Cuzol, P. Hellier, and E. Mémin, "A Low Dimensional Fluid Motion Estimator," *Int'l J. Computer Vision,* vol. 75, no. 3, pp. 329-349, 2007.

[14] A. Cuzol and E. Mémin, "A Stochastic Filter for Fluid Motion Tracking," *Proc. Int'l Conf. Computer Vision,* Oct. 2005.

[15] A. Cuzol and E. Mémin, "Vortex and Source Particles for Fluid Motion Estimation," *Proc. Fifth Int'l Conf. Scale-Space and PDE Methods in Computer Vision,* Apr. 2005.

[16] P. Del Moral, J. Jacod, and Ph. Protter, "The Monte-Carlo Method for Filtering with Discrete-Time Observations," *Probability Theory and Related Fields,* vol. 120, pp. 346-368, 2001.

[17] A. Doucet, S. Godsill, and C. Andrieu, "On Sequential Monte Carlo Sampling Methods for Bayesian Filtering," *Statistics and Computing,* vol. 10, no. 3, pp. 197-208, 2000.

[18] M. Farge, K. Schneider, and N. Kevlahan, "Non-Gaussianity and Coherent Vortex Simulation for Two-Dimensional Turbulence Using an Adaptive Orthogonal Wavelet Basis," *Physics of Fluids,* vol. 11, no. 8, pp. 2187-2201, 1999.

[19] G. Farnebäck, "Very High Accuracy Velocity Estimation Using Orientation Tensors, Parametric Motion, and Segmentation of the Motion Field," *Proc. Int'l Conf. Computer Vision,* pp. 5-26, 1999.

[20] P. Héas and E. Mémin, "3D Motion Estimation of Atmospheric Layers from Image Sequences," *IEEE Trans. Geoscience and Remote Sensing,* 2007.

[21] P. Héas, E. Mémin, and N. Papadakis, "Time-Consistent Estimators of 2D/3D Motion of Atmospheric Layers from Pressure Images," Technical Report 6292, INRIA, 2007.

[22] P. Héas, E. Mémin, N. Papadakis, and A. Szantai, "Layered Estimation of Atmospheric Mesoscale Dynamics from Satellite Imagery," *IEEE Trans. Geoscience and Remote Sensing,* vol. 45, no. 12, pp. 4087-4104, 2007.

[23] M. Isard and A. Blake, "Condensation—Conditional Density Propagation for Visual Tracking," *Int'l J. Computer Vision,* vol. 29, no. 1, pp. 5-28, 1998.

[24] P.E. Kloeden and E. Platen, *Numerical Solution of Stochastic Differential Equations.* Springer-Verlag, 1991.

[25] A. Leonard, "Vortex Methods for Flow Simulation," *J. Computational Physics,* vol. 37, 1980.

[26] C. Marchioro and M. Pulvirenti, "Hydrodynamics in Two Dimensions and Vortex Theory," *Comm. Math. Physics,* vol. 84, pp. 483-503, 1982.

[27] S. Méléard, "Monte-Carlo Approximations for 2D Navier-Stokes Equations with Measure Initial Data," *Probability Theory and Related Fields,* vol. 121, no. 3, pp. 367-388, 2001.

[28] R.N. Miller and L.L. Ehret, "Ensemble Generation for Models of Multimodal Systems," *Monthly Weather Rev.,* vol. 130, pp. 2313-2333, 2002.

[29] N. Papadakis and E. Mémin, "A Variational Method for Joint Tracking of Curve and Motion," Technical Report 6283, INRIA, Sept. 2007.

[30] N. Papadakis and E. Mémin, "A Variational Technique for Time Consistent Tracking of Curves and Motion," *Int'l J. Math. Imaging and Vision,* vol. 31, no. 1, pp. 81-103, 2008.

[31] P. Pérez, J. Vermaak, and A. Blake, "Data Fusion for Visual Tracking," *Proc. IEEE,* vol. 92, no. 3, pp. 495-513, 2004.

[32] D.T. Pham, J. Verron, and M.Ch. Roubaud, "A Singular Evolutive Extended Kalman Filter for Data Assimilation in Oceanography," *J. Marine Systems,* vol. 16, nos. 3/4, pp. 323-340, 1998.

[33] P. Ruhnau and C. Schnoerr, "Optical Stokes Flow Estimation: An Imaging-Based Control Approach," *Experiments in Fluids,* vol. 42, pp. 61-78, 2007.

[34] P. Ruhnau, A. Stahl, and C. Schnoerr, "On-Line Variational Estimation of Dynamical Fluid Flows with Physics-Based Spatio-Temporal Regularization," *Proc. 28th Ann. Symp. German Assoc. for Pattern Recognition,* Sept. 2006.

[35] P. Ruhnau, A. Stahl, and C. Schnoerr, "Variational Estimation of Experimental Fluid Flows with Physics-Based Spatio-Temporal Regularization," *Measurement Science and Technology,* vol. 18, pp. 755-763, 2007.

[36] J. Weickert and C. Schnoerr, "Variational Optic-Flow Computation with a Spatio-Temporal Smoothness Constraint," *J. Math. Imaging and Vision,* vol. 14, no. 3, pp. 245-255, 2001.

[37] J. Yuan, P. Ruhnau, E. Mémin, and C. Schnoerr, "Discrete Orthogonal Decomposition and Variational Fluid Flow Estimation," *Proc. Fifth Int'l Conf. Scale-Space and PDE Methods in Computer Vision,* Apr. 2005.

[38] J. Yuan, C. Schnoerr, and E. Mémin, "Discrete Orthogonal Decomposition and Variational Fluid Flow Estimation," *J. Math. Imaging and Vision,* vol. 28, no. 1, pp. 67-80, 2007.

Anne Cuzol received the PhD degree in applied mathematics from the University of Rennes, France, in 2006. She was a postdoctoral researcher in the Department of Computer Science, University of Copenhagen (DIKU) for eight months in 2007. She is currently an assistant professor at the European University of Brittany-UBS, Vannes, France. Her main research interests include stochastic models for motion estimation, tracking, and data assimilation for fluid flows images and environmental data.

Etienne Mémin received the PhD and habilitation degrees from Rennes I University in 1993 and 2003, respectively. His research activity focuses on motion analysis from image sequences. For several years, he has been investigating research on motion analysis for fluid flows. This concerns problems of motion estimation, segmentation, tracking, and characterization mainly for the study of geophysical fluids in environmental sciences or of industrial flows in experimental fluid mechanics. From 2003 to 2007, he headed a "Future and Emerging Technology" basic research European project entitled FLUID. Within this project, several methods for fluid flow motion estimation or the tracking of fluid state variables were proposed (see http://fluid/irisa.fr for demos, references, and codes). From February 2007 to August 2008, he worked as an invited researcher at the University of Buenos-Aires. He worked principally in the engineering faculty (FIUBA) and in the Center of Mathematics and Physics (CEFIMAS). During his stay, his works principally concerned the design of motion analysis techniques for Schlieren imaging, the estimation of reduced order dynamical systems through optimal control techniques, and the definition of regularization functions that comply with the statistics of turbulence. From 1994 to 1999, he worked as an assistant professor at the University of Bretagne Sud. Since 2000, he has been an assistant professor in the Department of Computer Science, Rennes I University. He is currently Research Director at INRIA.